Journal of The Electrochemical Society, **153** (12) B518-B526 (2006)
0013-4651/2006/153(12)/B518/9/$20.00 © The Electrochemical Society

Effect of Composition on the Photoelectrochemical Behavior of Anodic Oxides on Binary Aluminum Alloys

M. Santamaria,[a,*,z] F. Di Quarto,[a,*] P. Skeldon,[b,*] and G. E. Thompson[b,]**

[a]*Dipartimento di Ingegneria Chimica dei Processi e dei Materiali, Università di Palermo, Viale delle Scienze, 90128 Palermo, Italy*
[b]*Corrosion and Protection Centre, School of Materials, The University of Manchester, Manchester, Lancashire M60 1QD, United Kingdom*

The photoelectrochemical behavior of anodic films on Al alloys, containing titanium, tantalum, and tungsten (valve metals), has been studied as a function of alloy composition and anodizing conditions. Photocurrent spectroscopy has been used to get information on bandgap and the flatband potential values of different mixed oxides. Both insulator-like and semiconducting behavior has been observed for anodic oxides grown on Al-W and Al-Ti alloys dependent on alloy initial composition. Optical bandgap values, E_g^{opt}, of different oxides are in accordance with predictions based on the correlation between E_g^{opt} and the difference of electronegativities of the oxide constituents, indicating potential for tailoring solid state properties of ternary oxides.
 [DOI: 10.1149/1.2353809]

Manuscript submitted April 24, 2006; revised manuscript received July 27, 2006. Available electronically October 9, 2006.

Anodic films on valve metals alloys are of interest for investigating mechanisms of oxide growth; different works[1-6] have mainly focused their attention toward their morphology, structure, and composition to get insights on mechanism of anodic oxidation and ionic transport in "mixed oxides." Because these films are also of interest for possible application in electronics, for instance in metal-oxide semiconductor junctions[7-12] or in dye-sensitized photoelectrochemical and solid-state solar cells,[13,14] the possibility of controlled modification of the solid-state properties, such as bandgap, flatband potential, and dielectric constant, by use of "mixed oxides," is appealing from practical and theoretical viewpoints. This aspect becomes more important if we consider the prominent role of the solid-state properties of passive layers in controlling also the pitting behavior of metals and alloys.[15-17] Notably, it has been proposed that the bandgaps of crystalline binary oxides correlate with the electronegativities of their constituents, thus suggesting the possibility to predict the bandgaps of ternary oxides,[18-20] using an average electronegativity parameter for the cationic group and hence, tailoring of oxide properties. The correlation can apply also to amorphous oxides if account is taken of the influence of disorder on the optical bandgap value.[20,21]

In the present work, a study of the solid-state properties of anodic films on several Al alloys was carried out by using photocurrent spectroscopy (PCS) to measure their bandgap and flatband potential. The validity of the above mentioned correlation was tested to get information about its applicability and limits.

Experimental

Al-23 atom % Ti, Al-53 atom % Ti, and Al-34 atom % Ta alloys, prepared by physical vapor deposition, and Al-W alloys, containing 15, 23, and 77 atom % W, prepared by dc magnetron sputtering, were anodized either potentiodynamically, at 100 mV s^{-1}, or galvanostatically, at 5 mA cm^{-2} in either 0.1/0.01 M ammonium pentaborate electrolyte (ABE), of pH 8.5, or 0.01 N H_2SO_4 solution at room temperature. A three-electrode cell, with a saturated calomel electrode (SCE), and a two-electrode cell with a platinum cathode, were used in potentiodynamic and galvanostatic experiments, respectively.

The composition of Al-W alloys and anodic oxides grown on them were analyzed by Rutherford backscattering spectroscopy (RBS), using 1.83 MeV He^+ ions supplied by the Van de Graaff accelerator of the University of Paris. The scattered ions were detected at 165° to the direction of the incident beam. Data were interpreted by the RUMP program.

The photoelectrochemical setup and PCS have been described elsewhere.[19,20] Briefly, a 450 W UV-vis xenon lamp, coupled with a monochromator, irradiates the specimen through a quartz window in the anodizing cell. A two-phase, lock-in amplifier, with a mechanical chopper (chopping frequency 13 Hz), enables separation of the photocurrent from the total current. Photocurrent spectra are corrected for the relative photon efficiency of the light source at each wavelength so that the photocurrent yield in arbitrary current units is represented in the *y* axis.

Results

Kinetic behavior.— Potentiodynamic anodizing to 8 V of Al-Ti and Al-Ta alloys in ABE revealed usual behavior for growth of barrier oxide: an initial oxidation peak (or two peaks for Al-77 atom % W and Al-23 atom % W alloys) followed by a region of constant current density (Table I), between values for the similarly anodized relevant high purity metals (21-24), as shown for the Al-53 atom % Ti alloy (Fig. 1).

Under galvanostatic conditions, the voltage rose linearly with time for anodizing the alloys to 100 V in ABE (Table II), with films growing at high efficiency, except for the Al-53 atom % Ti alloy that evolved oxygen above 20 V, as occurs with titanium[22] and similar Al-Ti alloys.[23] For Al-W alloys, the voltage rose more slowly in H_2SO_4 solution than in ABE, due to loss of Al^{3+} ions to solution.

From previous work,[4,5] anodic films on Al-25 atom % Ti and Al-Ta alloys containing more than 32 atom % tantalum are relatively uniform amorphous oxides, based on units of alumina and the partner oxide. Furthermore, in Ref. 24 anodic films on Al-51 atom % Ti alloys are described as oxides, where the alloy components are distributed over the width virtually uniformly with a ratio Al^{3+}/Ti^{4+} close to unity. According to Ref. 24, X-ray photoelectron spectroscopy (XPS) data show that electrochemical oxidation of the alloy components is accompanied by formation of oxides, in which the chemical bond of Ti and Al with oxygen corresponds to the TiO_2 and Al_2O_3.

In Table III we compare the results of RBS analysis performed on anodic oxides on Al-W alloys. The composition depth profile revealed that thick anodic films grown in ammonium pentaborate electrolyte show a bilayered structure with an almost pure Al_2O_3

Table I. Current density relating to the anodizing of different Al alloys in 0.1 M ABE at 100 mV s^{-1} to U_F = 8 V(SCE).

Alloy	Al-23 atom % Ti	Al-53 atom % Ti	Al-34 atom % Ta
i (mA cm^{-2})	0.30 ± 0.05	0.40 ± 0.05	0.28 ± 0.05

* Electrochemical Society Active Member.
** Electrochemical Society Fellow.
z E-mail: santamaria@dicpm.unipa.it

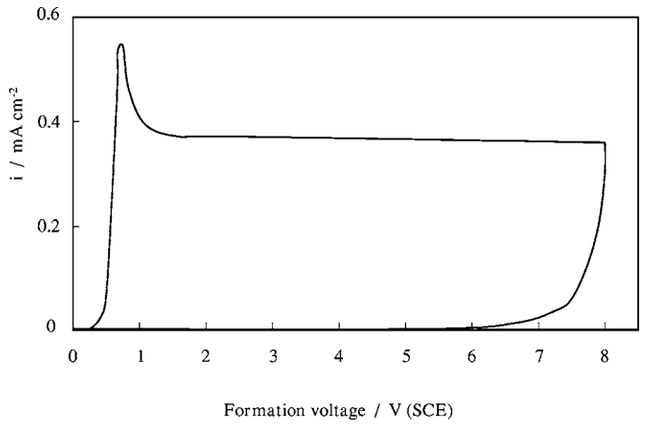

Figure 1. Current density vs formation voltage for anodizing Al-53 atom % Ti alloy at 100 mV s^{-1} in 0.1 M ABE at room temperature.

layer at the oxide/electrolyte interface, due to higher relative Al^{3+} migration rate with respect to W^{6+}. By anodizing in 0.01 N H_2SO_4, the outer layer is absent, due to higher solubility of alumina in acidic electrolyte, with the formation of a mixed Al-W oxide with the same composition of the inner layer of the anodic films grown in ABE. For each investigated alloy a W enrichment into the mixed oxide with respect to the base alloy has been revealed by RBS.

Photoelectrochemical behavior of thin films (U_F = 8 V).— In presenting the results on the photoelectrochemical behavior of the investigated mixed oxides, we group the anodic films according to their formation voltage in thin films (U_F = 8 V) and thick films ($U_F \geq$ 20 V). By compositionally averaging the anodizing ratios (i.e., the reciprocal of the electric field during the film growth), of pure anodic oxides of the alloy elements,[25] it is possible to calculate approximately the anodizing ratio of the alloys. According to this, oxide film thickness higher than 11 nm have been estimated for any anodized alloy at U_F = 8 V.

Photocurrent spectra were obtained for alloys anodized potentiodynamically to 8 V in 0.1 M ABE, with subsequent polarization at reduced voltage, U_E, except for the Al-15 atom % W alloy for which no photocurrent was detected. The example of the Al-53 atom % Ti alloy for U_E = 2 V (SCE) (Fig. 2a), indicates an optical bandgap of 3.55 eV (Fig. 2b) derived according to the relationship

$$(I_{ph}h\nu)^{n/2} \propto (h\nu\text{-}E_g^{opt}) \quad [1]$$

where, for photon energy in the vicinity of bandgap, I_{ph} is proportional to the light absorption coefficient. As usual, $h\nu$ is the photon energy and n = 1 holds for indirect (nondirect for amorphous films) optical transitions.[19] An Urbach tail occurs at lower photon energies (Fig. 2c), which can be due to optical transitions involving localized states in the mobility gap of amorphous oxides. The end of the linear part in the Urbach plot can be assumed as a measure of the mobility gap in amorphous materials.[19] E_g^{opt} values, estimated according to Eq. 1, for all films depend strongly on the types and amounts of the oxide constituents (Table IV). Note that the bandgap value of 3.68 eV for the Al-77 atom % W alloy anodized in H_2SO_4 solution, reduced to 3.48 eV after 1 h of polarization in the same electrolyte.

Table III. Tungsten atomic fraction, x_W, (on the base of cations only) for anodic films grown at 5 mA cm^{-2} on sputtered Al-W alloys.

	x_W in the inner layer	x_W
Alloy	0.01 M ABE	0.01 H_2SO_4
Al-15 atom % W	0.21 (U_F = 100 V)	0.22 (U_F = 50 V)
Al-23 atom % W	0.29 (U_F = 100 V)	0.29 (U_F = 80 V)
Al-77 atom % W	—	0.86 (U_F = 100 V)

Only anodic photocurrents have been detected in the case of anodic oxides on Al-53 atom % Ti and Al-77 atom % W, suggesting a semiconducting n-type behavior of these films. The anodic photocurrent is due to water oxidation by holes photogenerated in the valence band of the oxides. In contrast, anodic and cathodic photocurrents have been revealed for anodized Al-23 atom % Ti, Al-34 atom % Ta, and Al-23 atom % W, indicating the formation of insulating layers, for which the photocurrent sign depends on the direction of the electric field within the film.[19] The cathodic photocurrent is associated to the reduction of water and/or oxygen by the electron photogenerated in the conduction band of the oxides. In Fig. 3 we report the current vs time curves in the dark and under irradiation with different wavelengths for two electrode potentials relating to an oxide grown on Al-23 atom % Ti. The photocurrent is anodic at −0.5 V (SCE) and cathodic at −0.8 V (SCE), indicating a V_{FB} in between these values. In Fig. 4 the cathodic photocurrent spectrum relating to anodic films grown on Al-23 atom % Ti, recorded at U_E = −1 V(SCE), is shown. Its shape is very similar to that of the anodic ones and a bandgap of 3.85 eV can be estimated by assuming nondirect optical transitions, in agreement with the values obtained from the anodic spectra. A similar behavior has been showed by anodic films on Al-23 atom % W.

In contrast, in the case of anodic film on Al-34 atom % Ta the shape of the photocurrent spectra is dependent on the polarizing voltage. In Fig. 5 we report the photocurrent intensity and its phase angle for a film grown to 8 V (SCE) on this alloy, polarized at U_E = −0.5 V (SCE). At short wavelengths ($\lambda < 320$ nm) the anodic transients give an onset for the interband transitions of 4.35 eV, while at longer wavelengths a steady state cathodic photocurrent is recorded (see inset). A rapid change in the phase angle marks the change of the photocurrent sign. At lower polarizing voltage (U_E = −0.8 V/SCE) only cathodic photocurrent is present (see Fig. 6). A bandgap value almost coincident with that estimated at 2 V (SCE) can be derived from the high energy region by assuming nondirect optical transitions. Cathodic photocurrents at energies below E_g^{opt} is attributed to electron photoemission from the Fermi level of the alloy to the oxide conduction band, with an internal photoemission threshold energy E_{th} = 1.4 ± 0.05 eV (Fig. 7) estimated according to Fowler law

$$(I_{ph})^{0.5} = \text{const}(h\nu\text{-}E_{th}) \quad [2]$$

The external electron photoemission (from the alloy Fermi level to the electrolyte) is excluded owing to the large film thickness.

The knowledge of the bandgap and of the cathodic photoemission threshold for the Al-Ta mixed oxide allows to get the energetic sketch of Fig. 8, which has been derived by assuming for

Table II. Slopes of galvanostatic curves for film grown to 100 V at 5 mA cm^{-2} in 0.01 M ABE.

Alloy	Al-23 atom % Ti	Al-53 atom % Ti	Al-34 atom % Ta	Al-15 atom % W	Al-23 atom % W	Al-77 atom % W
dV/dt (V s^{-1})	1.90 ± 0.05	1.70 ± 0.10 1.25 ± 0.05[a]	2.00 ± 0.10	2.30 ± 0.10	1.85 ± 0.10	1.75 ± 0.10

[a] $U_F \geq$ 20 V

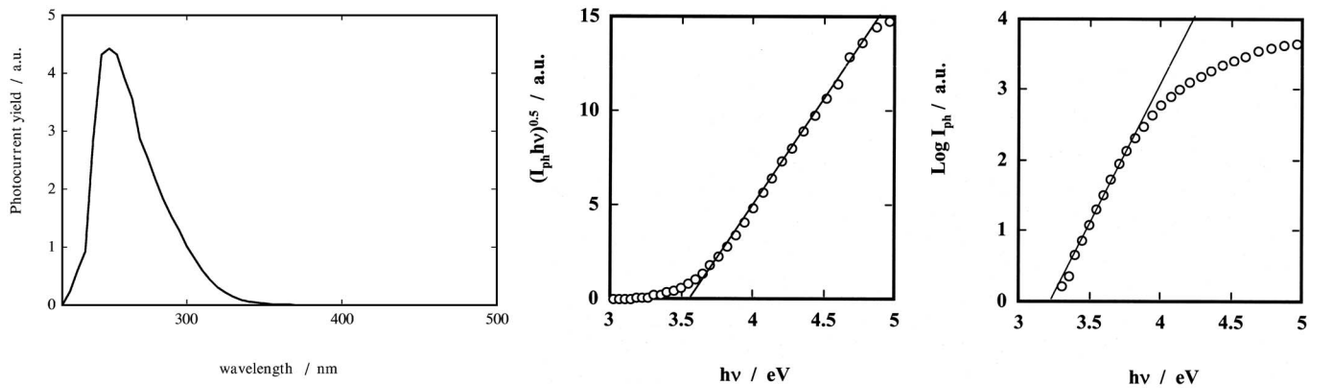

Figure 2. (a) Photocurrent spectrum relating to an anodic film grown to 8 V(SCE) on Al-53 atom % Ti at 100 mV s^{-1} in 0.1 M ABE and polarized in the same electrolyte at U_E = 2 V(SCE). (b) $(I_{ph}h\nu)^{0.5}$ vs $h\nu$ plot and (c) Urbach tail.

Al-34 atom % Ta a work function between those reported for Al and Ta (according to Ref. 26, 4.20 and 4.15 eV, respectively). A cathodic photocurrent tail at long wavelengths is usually observed with insulating wide bandgap oxides such as ZrO_2, Al_2O_3, and Ta_2O_5 at electrode potentials near V_{FB},[27-29] and it has been reported also for passive Mo-79 atom % Ta.[21]

To get further information on the semiconducting or insulating behavior of the investigated films, photocurrent vs electrode potential curves (photocharacteristics) under monochromatic light have been recorded. By polarizing toward the cathodic direction at a scan rate, v_{scan}, of 10 mV s^{-1}, an inversion of the photocurrent sign was revealed for anodized Al-23 atom % Ti (Fig. 9), Al-34 atom % Ta and Al-23 atom % W alloys, thus confirming the formation of insulating oxides. The inversion potentials, which are a rough estimate of the flatband potential for insulating layers,[19] are summarized in Table V. In contrast, no inversion of photocurrent sign was evidenced for anodic films on Al-53 atom % Ti and Al-77 atom % W alloys in agreement with a n-type semiconducting behavior of mixed oxides (Fig. 10), reminiscent of the behavior of TiO_2 and WO_3, respectively.

For these films a different approach has been followed to estimate their flatband potential. For the n-type oxide on Al-77 atom % W alloy, a V_{FB} = 0.05 ± 0.1 V(SCE) at pH 2 is assumed (see Fig. 10), coincident with average potential of the zeroing of photocurrent in the photocharacteristics recorded at different wavelengths in 0.01 N H_2SO_4 solution, where a chemically stable film is formed. The V_{FB} value could be adjusted to pH 8.5 using the relationship

$$V_{FB} = \text{const.} - 0.059\ \text{pH} \qquad [3]$$

usually reported to hold for oxide semiconductors.[30] After correction for the solution pH, a V_{FB} = −0.28 ± 0.1 V(SCE) was estimated for the mixed oxide on Al-77 atom % W in ABE solution. The presence of units of alumina in mixed oxide on both the investigated Al-W alloys shifts V_{FB} toward the cathodic direction with respect to the flatband potential of a-WO_3, for which a V_{FB} = 0.40 ± 0.1 V (SCE) at pH 0 is reported in Ref. 31, which becomes −0.10 V(SCE), once corrected by Eq. 3 at pH 8.5. The larger shift of V_{FB} value toward cathodic potentials for film grown on lower alloyed Al-W sputtered layer is also in agreement with the theoretical expectation.

In the case of anodized Al-53 atom % Ti alloy the beginning of

Table IV. Optical bandgap values, average electronegativities, χ_M and ΔE_{am} of anodic films grown to 8 V (SCE) at 100 mV s^{-1} on different Al alloys.

Sample/atom %	Anodizing electrolyte	E_g^{opt}/eV	χ_M	ΔE_{am}/eV
Al-23 atom % Ti	0.1 M ABE	3.86	1.536	0.14
Al-53 atom % Ti	0.1 M ABE	3.55	1.583	0.08
Al-34 atom % Ta	0.1 M ABE	4.30	1.50	0.39
Al-15 atom % W	0.01 N H_2SO_4	—	1.53	—
Al-23 atom % W	0.01 N H_2SO_4	4.05	1.546	0.38
Al-77 atom % W	0.01 N H_2SO_4	3.68	1.654	0.57

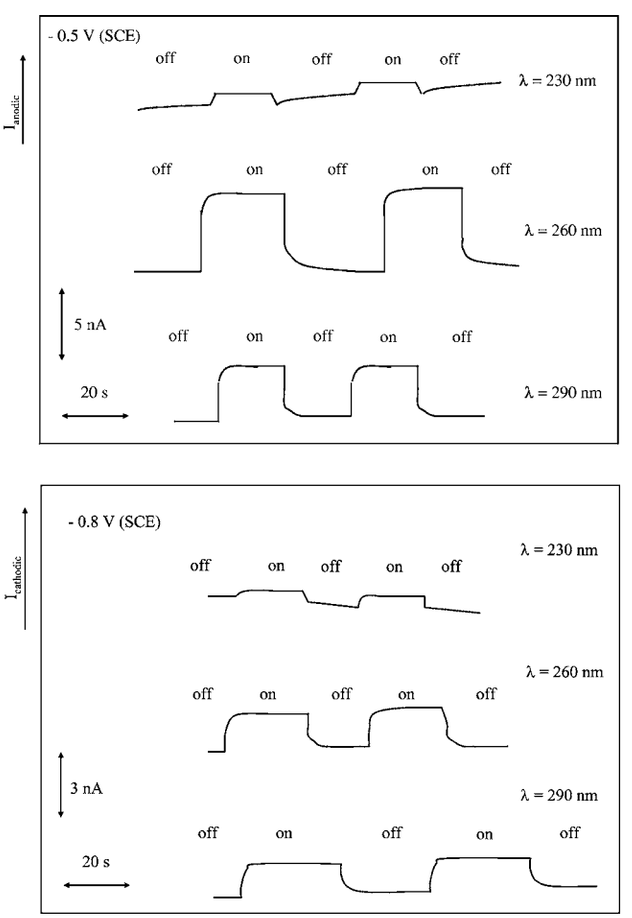

Figure 3. Total current vs time for an anodic film grown to 8 V(SCE) on Al-23 atom % Ti at 100 mV s^{-1} in 0.1 M ABE, in the dark (off) and under irradiation (on) at different wavelengths. Sol: 0.1 M ABE.

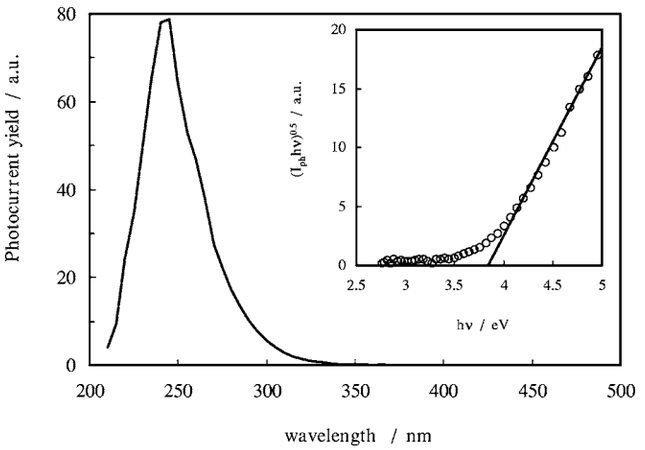

Figure 4. Photocurrent spectrum relating to an anodic film grown to 8 V(SCE) on Al-23 atom % Ti at 100 mV s^{-1} in 0.1 M ABE and polarized in the same electrolyte at $U_E = -1.0$ V(SCE). Inset: estimation of the optical bandgap by assuming nondirect optical transitions.

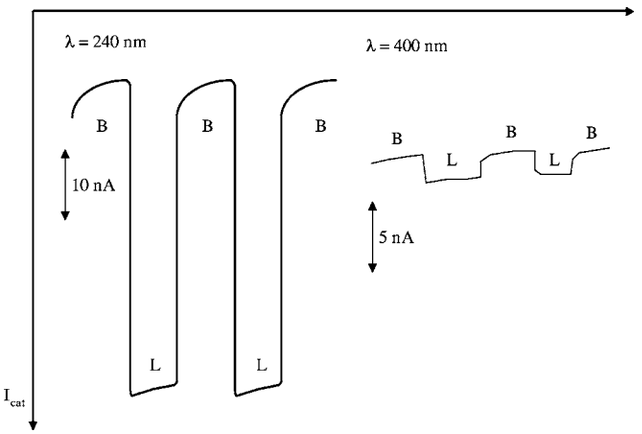

Figure 6. Total current vs time for an anodic film grown to 8 V(SCE) on Al-34 atom % Ta at 100 mV s^{-1} in 0.1 M ABE, in the dark (off) and under irradiation (on) at different wavelengths at $U_E = -0.8$ V(SCE). Sol: 0.1 M ABE.

a cathodic process at electrode potentials more positive than V_{FB} hampered to get the region of zeroing photocurrent. Thus, in this case, to estimate the flatband potential of the oxide the photocharacteristics were fitted according to a power law, $(I_{ph})^n \propto U_E$ (see Fig. 11), and a V_{FB} coincident with the extrapolated potential of zero photocurrent, V^*, has been assumed.[19] The values of n and V^* obtained at each wavelength are reported in Table VI. The disclosed supralinear behavior ($n < 1$) in a large potential range (Fig. 11), as well as the dependence of n on the wavelength, has been attributed to the presence of initial (geminate) recombination effects of injected photocarriers. Geminate recombination effects can occur if the thermalization length of the photogenerated electron-hole pairs is too short to prevent some recombination of photocarriers, and it is typical in amorphous material, owing to a low mobility of electron carriers in localized states near the mobility gap.[19]

By averaging the V^* values for different wavelengths, a $V_{FB} \cong -0.55 \pm 0.05$ V(SCE) has been assumed for the anodic oxide on the Al-53 atom % Ti alloys. V_{FB} estimated for the anodic film on Al-53 atom % Ti alloy is more cathodic than that reported for thin anodic films on a Al-50 atom % Ti alloy,[32] obtained by fitting the photocharacteristics in a rather limited region of electrode potentials with $n = 2$. Such a value of n, usually predicted for crystalline semiconductors, occurs with amorphous semiconductors with appropriate distributions of states within the gap and collection lengths.[19] However, reliable information from photocharacteristics is best achieved from a full investigation of the dependence of I_{ph} on both U_E and λ, accounting for the possible amorphous nature of oxides. For comparison with results pertaining Al-Ti alloys, photocharacteristics relating to anodic oxides formed to 8 V at 100 mV s^{-1} on pure cast titanium in 0.1 M ABE have been recorded. The best fitting procedure indicated $V^* = -0.35 \pm 0.05$ V (SCE) (see Table VI), thus suggesting that the presence of units of alumina in the mixed oxide causes shifts V_{FB} toward the cathodic direction with respect to V_{FB} of TiO_2. Moreover, the trend of the exponent n suggests an increase in the amorphous nature of the mixed film, owing to the presence of the partner oxide.

For anodized Al-34 atom % Ta alloy the estimated V_{fb} (−0.60 V/SCE, see Table V) is more positive than that reported for thin films of anodic tantala at the same pH ($V_{FB} = -1.05$ V/SCE from data in Ref. 27). On the other hand, for the Al/Al_2O_3 in ammonium tartrate electrolyte at pH 6.7, a zero anodic photocurrent potential of −0.70 V (SCE) has been estimated for anodic alumina film grown in such an electrolyte.[33] Thus, by means of Eq. 3 a

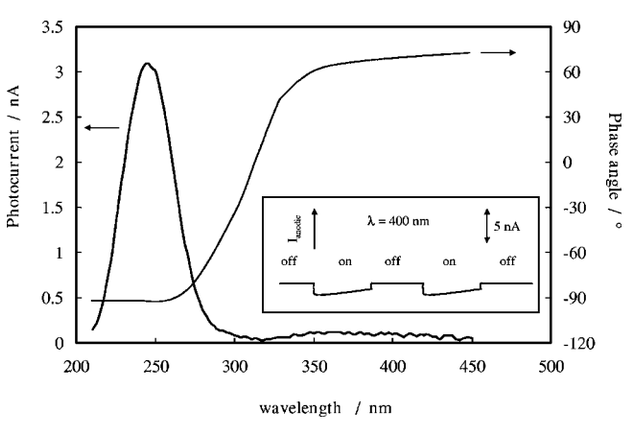

Figure 5. Photocurrent intensity and its phase angle vs wavelength for an anodic film grown to 8 V(SCE) on Al-34 atom % Ta at 100 mV s^{-1} in 0.1 M ABE, recorded by polarizing the electrode in 0.1 M ABE at $U_E = -0.5$ V(SCE). Inset: total current in the dark and under irradiation.

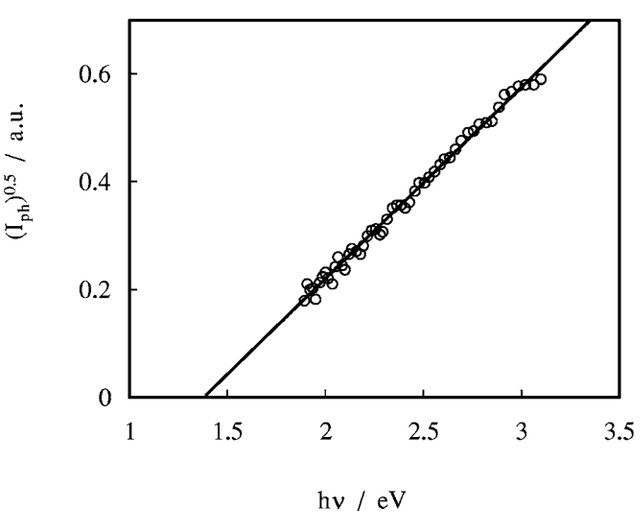

Figure 7. Fowler plot at $U_E = -1.3$ V(SCE) for the anodic film of Fig. 5. Sol: 0.1 M ABE.

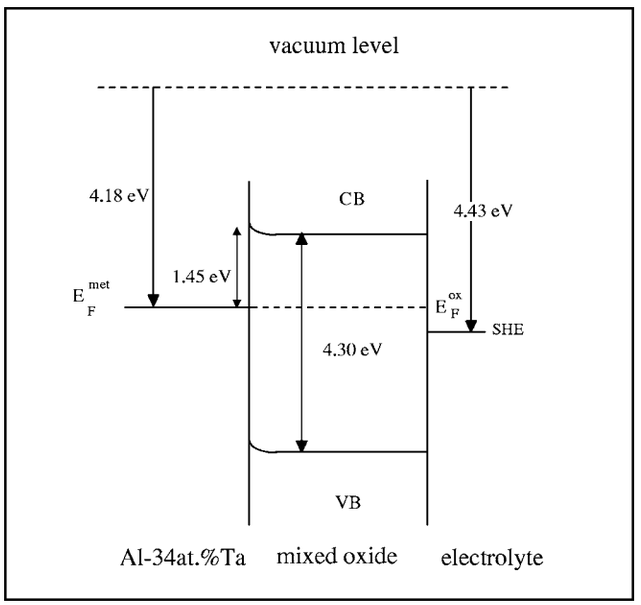

Figure 8. Energy scheme of metal/anodic film/electrolyte junction for anodized Al-34 atom % Ta.

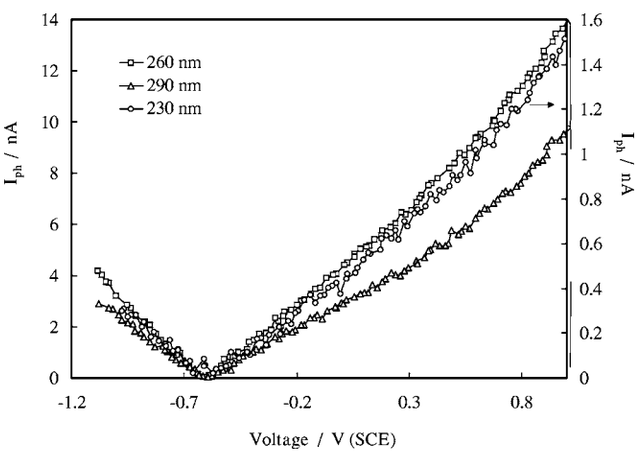

Figure 9. I_{ph} vs U_E curves recorded by irradiating at different wavelengths anodic films grown to 8 V(SCE) at 100 mV s^{-1} in 0.1 M ABE on different Al-23 atom % Ti. Sol: 0.1 M ABE and v_{scan} = 10 mV s^{-1}.

Table V. Photocurrent sign inversion potentials of anodic films grown to 8 V(SCE) in 0.1 M ABE at 100 mV s^{-1}. Sol: 0.1 M ABE and v_{scan} = 10 mV s^{-1}.

Base alloy	Al-23 atom % Ti	Al-34 atom % Ta	Al-23 atom % W
V_{inv}/V(SCE)	−0.57 ± 0.03	−0.60 ± 0.05	−0.37 ± 0.03

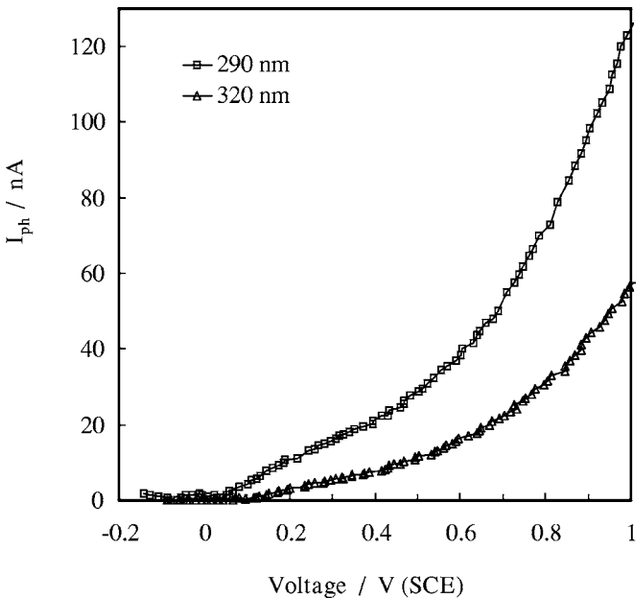

Figure 10. I_{ph} vs U_E curves recorded by irradiating at different wavelengths an anodic film grown to 8 V(SCE) at 100 mV s^{-1} in 0.01 N H_2SO_4 on Al-77 atom % W. Sol: 0.01 N H_2SO_4 and v_{scan} = 10 mV s^{-1}.

flatband potential of −0.80 V(SCE) can be tentatively attributed to anodic oxide film in ABE solution at pH 8.5. It comes out that the flatband potential of anodic oxide grown on Al-34 atom % Ta is more anodic than that of both pure partner oxides.

The results show that V_{FB} has a complex dependence on the oxide composition, which is expected by considering that V_{fb} depends not only on the nature of the oxide but also on the nature (n- or p-type) and concentration of doping. Thus, it is really difficult to relate quantitatively the flatband potential to the oxide composition. In Ref. 16, a correlation was proposed between V_{FB}, isoelectric point and bandgap of metal oxides. Accordingly, a more cathodic V_{FB} is expected with increasing E_g^{opt} and pH of zero charge. Because increased presence of units of alumina increases the bandgap of mixed oxides with respect to the corresponding partner oxide, and is also

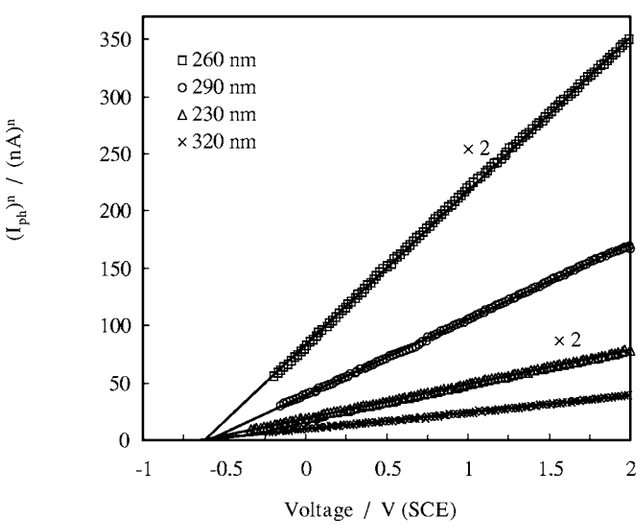

Figure 11. $(I_{ph})^n$ vs U_E for an anodic film grown to 8 V(SCE) on Al-53 atom % Ti at 100 mV s^{-1} in 0.1 M ABE. Sol: 0.1 M ABE and v_{scan} = 10 mV s^{-1}.

Table VI. Exponent *n* and extrapolated zero photocurrent potential, V^*, obtained for anodic films on Ti and Al-53 atom % Ti grown to 8 V(SCE) in 0.1 M ABE at 100 mV s^{-1}. Sol: 0.1 M ABE and v_{scan} = 10 mV s^{-1}.

Base alloy	λ / nm	*n*	V^*/V(SCE)
Ti	230	1.35	−0.38
	260	1.125	−0.35
	290	0.95	−0.31
Al-53 atom % Ti	230	0.95	−0.63
	260	0.90	−0.62
	290	0.80	−0.59
	320	0.70	−0.61

expected to increase the pH_{pzc},[16] the estimated V_{FB} for Al-Ti, Al -W alloys follow the proposed trend,[16] while the estimated V_{FB} for anodized Al-34 atom % Ta alloys does not show the predicted dependence.

Photoelectrochemical behavior of thick films ($U_F \geq 20$ V).— For the Al-34 atom % Ta alloy, E_g^{opt} reduces with increased forming voltage, and hence oxide thickness, as indicated by the bandgap values reported in Table VII. At each thickness, a tailing in the anodic photocurrent spectrum was visible under anodic polarization, probably arising from the presence of localized states near the mobility gap. However, a less probable photoinjection of holes from the metal to the valence bandedge cannot be excluded. Furthermore, a photocurrent inversion, with stationary cathodic I_{ph}, suggests insulating behavior of formed film. An electron photoinjection process operates under cathodic polarization, with the threshold energy of Table VII, estimated according to Fowler law. We stress that an increasing Fowler threshold was obtained under constant cathodic potential (U_E = −1.0 V/SCE) but increasing film thickness (i.e., anodizing voltage). Notably, a thermal oxide formed for 3.5 h in oxygen on the Al-34 atom % Ta alloy at 600°C had the lowest E_g^{opt} and the same Fowler threshold. The current-voltage response at 100 mV s^{-1} confirmed formation of a barrier film having a thickness equivalent to that of an anodic film grown up to 80 V.

For anodic films formed on Al-23 atom % Ti, an E_g^{opt} slightly decreasing with increasing formation voltage (i.e., thickness) has been found. A bandgap value of 3.75 eV has been estimated for a film grown at 100 mV s^{-1} to 90 V. Nevertheless, the effect of increasing formation voltage can be cancelled by increasing the growth rate: E_g = 3.85 eV is obtained for anodic films formed up to 90 V at 1.9 V s^{-1}.

For the Al-53 atom % Ti alloy, E_g^{opt} depends upon the formation voltage (Table VIII), with E_g^{opt} similar to that reported for TiO_2 for formation voltage of 100 V. For both anodized Al-Ti alloys, anodic photocurrent spikes occur for thicker films as U_E is moved toward the cathodic direction, which hinders estimate of V_{FB}.

Table VII. Bandgap and Fowler thresholds of oxide films grown on Al-34 atom % Ta alloys. Polarizing electrolyte: 0.1 M ABE.

Formation voltage	Growth conditions	E_g^{opt}/eV	E_{th}^{exp}/eV	E_{th}^{corr}/eV
Air formed film	—	4.35	—	—
8 V (SCE)	100 mV s^{-1} in 0.1 M ABE	4.30	1.45	1.54
22 V	100 mV s^{-1} in 0.1 M ABE	4.25	1.55	1.61
80 V	100 mV s^{-1} in 0.1 M ABE	4.15	1.64	1.67
—	Thermal treatment (3.5 h at T = 600°C)	3.96	1.56	1.59

Table VIII. Bandgap values of anodic oxide grown on Al-53 atom % Ti as a function of the anodizing conditions. Polarizing electrolyte: 0.1 M ABE.

Formation voltage	Anodizing conditions	E_g^{opt}/eV
8 V (SCE)	100 mV s^{-1} in 0.1 M ABE	3.55
15 V	100 mV s^{-1} in 0.1 M ABE	3.54
40 V	100 mV s^{-1} in 0.1 M ABE	3.48
80 V	100 mV s^{-1} in 0.1 M ABE	3.38
100 V	5mA cm^{-2} in 0.01 M ABE	3.25

Similar to thinner films photocurrents were absent for thicker films formed up to 50 V in either ABE or H_2SO_4, for anodized Al-15 atom % W alloy. For the Al-23 atom % W alloy, E_g^{opt} values of 4.0 ± 0.05 eV were determined for films formed to $V_{FB} \leq 60$ V in H_2SO_4 solution and to 100 V in ABE, with higher E_g^{opt} values pertaining to the thinner film.

For the Al-77 atom % W alloy, E_g^{opt} decreases with increasing formation voltage, reaching a value of 3.34 eV for anodizing voltage equal to 100 V in H_2SO_4 solution. Analogously to thin film the thicker oxide film on Al-23 atom % W and Al-77 atom % W alloys behave like insulators and n-type semiconductors, respectively.

Discussion

The experimental findings suggest that anodizing of aluminum-valve metal alloys produces insulating or semiconducting oxides, depending on the nature and relative amounts of the alloy constituents. Amorphous anodic oxides on electropolished aluminum are insulating with a wide ($E_g \geq 6.3$ eV) bandgap,[34] while thin hydroxide layers having lower bandgap ($E_g \cong 3.0$ eV) can also be formed on mechanically treated Al surface.[34] Anodic films on Al-23 atom % Ti, Al-23 atom % W, and Al-34 atom % Ta alloys are insulators, while anodic films on the more highly alloyed Al-53 atom % Ti and Al-77 atom % W alloys are n-type semiconductors, correlating with the n-type nature of TiO_2 and WO_3, having bandgaps of 3.2 eV[24] and 2.7 eV,[35] respectively.

Previous work[18] proposed that the optical bandgaps of crystalline oxides, M_xO_y, are proportional to the square of the electronegativity difference of their constituents, based on the assumption of a direct relation between the bandgap and the single M-O bond energy, obtained from the Pauling equation for the single bond energy.

The following fitting equations have been suggested to apply[18-20] to amorphous sp and d metal oxides, respectively, with few exceptions

$$\text{sp)} \quad E_g^{opt}\text{-}\Delta E_{am}(\text{eV}) = 2.17(\chi_M\text{-}\chi_O)^2 - 2.71 \qquad [4]$$

$$\text{d)} \quad E_g^{opt}\text{-}\Delta E_{am}(\text{eV}) = 1.35(\chi_M\text{-}\chi_O)^2 - 1.49 \qquad [5]$$

The rare earth metal oxides seem to follow the d-metal oxide correlation.[20] χ_M and χ_O are the electronegativities of metal and oxygen, respectively, and ΔE_{am} is a parameter which takes into account the influence of amorphous nature on the bandgap of the oxides. E_g^{opt} is the mobility gap in amorphous oxide according to Fig. 12. The term ΔE_C and ΔE_V are a measure of the extent of localization of electronic states near the conduction and valence band mobility edges, respectively. A value of 0.20 eV has been suggested as typical for ΔE_C and ΔE_V, owing to lattice disorder in otherwise stoichiometric crystal.[36] According to Fig. 12, $\Delta E_{am} = 0$ for crystalline oxides, when $E_g^{opt} = E_g$, while increasing values are expected (up to ~0.5 eV) if the lattice disorder affects both the mobility edges in a similar manner.

For mixed oxides $A_aB_bO_y$, it has been suggested that the previous correlation are still valid provided that the average single bond energy is estimated taking into account the contributions of both, A and B, cations of the oxide trough an average cationic electronegativity parameter, χ_M, given by

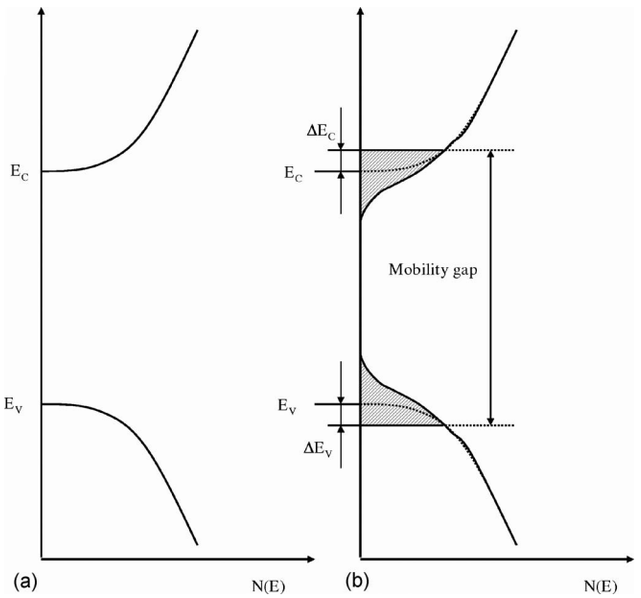

Figure 12. Density of states, $N(E)$ as a function of energy E for (a) crystalline and (b) amorphous semiconductors. Dotted area indicates localized states. ΔE_C and ΔE_V are band tails due to disorder.

$$\chi_M = x_a\chi_A + x_b\chi_B \quad [6]$$

where A and B are the metals of the oxide, and $x_{a,b}$ their cationic fractions. For mixed sp-sp metals oxides or mixed d-d metals oxides the correlation seems to hold without restriction[20] for any A/B ratio. In the presence of mixed sp-d-metals oxides the proposed correlation must be used with some caution. It has been reported in a previous paper that provided a minimum amount ($\geq$25%) of d-metal cation is present in the mixed oxide the d-metal oxide correlation is able to explain the trend in measured E_g^{opt} value of mixed sp-d metals oxides as a function of average electronegativity parameter defined according to Eq. 6. Moreover if the difference in the electronegativity parameter of d and sp metal is higher than 0.5 the bandgap value is usual very near to the bandgap of the d metal oxides.[18]

It is within the aim of this work to test also the limit of validity of proposed correlation for mixed sp-d metal oxides. In Table IV we report the ΔE_{am} values estimated by comparing the experimental E_g^{opt} with the theoretical estimate according to Eq. 5 and with χ_M calculated by means of Eq. 6. The electronegativities of pure metals are those reported by Pauling[37] with exception of titanium, whose χ has been calculated as the arithmetic mean between the electronegativity of Ti obtained by Eq. 5 from the bandgap values of rutile and anatase,[38] and its value is in the range of uncertainty proposed by Pauling. ΔE_{am} has been estimated assuming an Al-partner metal ratio equal to that of the base alloy. Nevertheless, the composition of films on valve metal alloys depends on the relative migration rates of the cation species of the oxides as well as on the stability of surface layer in the different electrolyte used in the formation process. For Al-23 atom % Ti, Al-53 atom % Ti, and Al-34 atom % Ta alloys, similarity of rates and good stability of surface layer in ABE solution result in uniform oxides with cation fractions approximating to the alloy composition, allowing a direct estimation of E_g^{opt} from Eq. 5 and 6. For such oxides formed to 8 V (SCE), the calculated ΔE_{am} values (see Table IV) agree with the theoretical expectations.[36] The larger value measured for the Al-Ta alloy is unsurprising, as amorphous alumina and tantala films form under the current growth conditions, while partially crystalline oxides occur for titanium.[38]

With increased formation voltage, E_g^{opt} for the Al-Ta mixed oxide decreases which, according to Eq. 5 and 6, can only be related to a reduced ΔE_{am}, as the Pauling electronegativities of aluminum and tantalum are equal.[37] This suggestion is further supported by a low E_g^{opt} of the thermal oxide on the Al-34 atom % Ta alloy (Table VII), which is very near to that calculated from Eq. 5 for crystalline Ta_2O_5.[39] A further support to this suggestion comes from the dependence of the Fowler's threshold value on the film thickness. As reported in Table VII a steadily increasing E_{th} value with increasing film thickness was measured at constant cathodic polarizing voltage. This increase is compatible with the effect of lowering of Schottky barrier, $\Delta\phi_B$, at the metal/oxide interface, due to the image force, which is dependent on the electric field, E, according to[33]

$$\Delta\phi_B = \phi(E = 0)\text{-}\phi(E) = 3.84\ 10^{-4}\sqrt{\frac{E}{\varepsilon_{opt}}} \quad [7]$$

where $\Delta\phi_B$ is in eV and E is in V cm^{-1}. ε_{opt} is the dielectric constant at high frequency, assumed equal to the squared refractive index, n_{ox}^2. The electric field can be estimated as a function of the anodizing ratio, A, and formation voltage, U_F, as

$$E = \frac{U_E - V_{FB}}{AU_F} \quad [8]$$

By assuming $n_{ox} = 1.70$ [22] and for the mixed oxide an anodizing ratio of $A = 14$ Å V^{-1}, averaged between those reported for pure alumina and tantala,[25] we estimated the zero field Fowler thresholds at different thickness reported in Table VII for electron photoemission from the alloy Fermi level to the conduction band mobility edge of mixed oxide. After correction, we still observed a difference of about 0.1 eV in the cathodic photoemission threshold values, at different thickness, which could be attributed to the lack of a sharp mobility edge typical of amorphous material.

On the other hand, note that the difference in E_g^{opt} values of 80 V anodic film and corresponding thermal oxide is still about twice the difference in photoemission threshold. This finding agrees with $\Delta E_{am} = \Delta E_C + \Delta E_V$ and $\Delta E_C \cong \Delta E_V \cong 0.1$ eV, as sketched in Fig. 12. The decrease of E_g^{opt} with increasing thickness agrees with the hypothesis that anodic thicker films display a reduction in the extent of localized DOS near the mobility edges. This is also confirmed by the dependence of the photocurrent from energy in the Urbach region, i.e., for energy lower than the optical bandgap of the films, where the photocurrent can be generated by absorption involving one or both the band tails. In this region the dependence of light absorption coefficient, α, follows

$$\alpha = \alpha_0 e^{-\frac{E_0 - h\nu}{E_U}} \quad [9]$$

where E_0, the Urbach mobility gap, marks the end of linearity in the ln α vs $h\nu$ plot and E_U is a measure of the width of band tails, i.e., the extent of DOS localization near the mobility edge. E_U ranging between 0.094 and 0.055 eV were obtained for thin (8 V/SCE) and thick (80 V) film on Al-34 atom % Ta, respectively, thus suggesting larger tails for thinner film.

It comes out that the tendency of anodic Ta_2O_5 to become more ordered with increasing anodizing voltage, although still present in mixed oxide, is strongly counteracted by the amorphous nature of aluminum oxide. In fact E_g^{opt} values of mixed oxide appreciably larger ($>$0.2 eV) than that measured for pure anodic oxide on Ta metal[27] agrees with the suggested amorphizing influence of aluminum oxide. Moreover by comparing the bandgap value of thermal Ta_2O_5 with the E_g^{opt} values in Table VII we suggest that amorphous mixed oxide is formed at any thickness during anodic oxidation of Al-34 atom % Ta alloy while a quasi-crystalline mixed oxide is formed by thermal oxidation in analogy with similar finding on pure Ta metal.[40]

As for the estimate of flatband potential, it seems evident that the inversion photocurrent potential is more anodic than any expected value if we consider that both Ta_2O_5 and Al_2O_3 display more ca-

thodic V_{FB} values than the inversion photocurrent potential of the mixed oxide. A rationale for this discrepancy could be traced to the fact that under illumination a surface trapping of photogenerated hole could occur in localized states near the valence band mobility edge with a consequent shift of the bandedges. Such a finding, previously observed on other amorphous anodic oxides (Nb_2O_5 and TiO_2), deserves further investigation to get reliable information on V_{FB} of anodized Al-34 atom % Ta.

Increased film thickness has the same effect for the Al-23 atom % Ti alloy, with respective E_g^{opt} values of 3.86 and 3.75 eV for thin and thick films formed at 100 mV s^{-1}. The increased thickness increases the crystallinity of the oxide as confirmed by the higher bandgap value (3.85 eV) measured for thick (V_f = 90 V) films formed at higher growth rate (1.9 V s^{-1}). The value of ΔE_{am} for thin film is comprised between 0.11 eV and 0.16 eV depending on the value of electronegativity parameter we choose for titanium (χ_{Ti} = 1.676 for rutile, χ_{Ti} = 1.636 for anatase). This value is lower than the previous one and is in agreement with the tendency of TiO_2 film to crystallize during the anodizing process since low voltages and more easily as lower the growth rate is.[38]

For the Al-53 atom % Ti alloy, E_g^{opt} decreases with increase of forming voltage (Table VIII). In this case a decrease in ΔE_{am} cannot explain the photocurrent spectra behavior of the films, since $\Delta E_{am} \leq 0$ is required to fit results using Eq. 5 and 6, as the formation voltage increases. In this case, lower E_g^{opt} values can arise from the formation of anodic films enriched in Ti with respect to the base alloy, more pronounced as the formation voltage increases with the formation of titania outer layer, with E_g^{opt} of 3.25 eV, at high voltages. The presence of an almost pure TiO_2 outer layer on anodized Al-74 atom % Ti has been reported in Ref. 22 due to a faster migration rate of Ti^{4+} with respect to Al^{3+}.

For the Al-W alloys, RBS indicates an outer alumina layer forms during the anodizing in ABE, but not in H_2SO_4 solution of low pH. Using RBS data compositions (Table III) together with Eq. 5 and 6, for thick films ΔE_{am} values of 0.38 and 0.30 eV were obtained for mixed oxides with tungsten fractions of 0.29 and 0.86, respectively, in agreement with theoretical expectation and higher than those estimated for other thick mixed oxides. Such finding agrees with the above mentioned suggestion based on the tendency to crystallize of each partner, the scarce tendency to crystallize of anodic WO_3 and Al_2O_3 being well known.

Finally, the mechanism of growth of mixed film and the relative mobility of different cations as a function of metal-oxygen bond[41] can help to explain the differences in E_g^{opt} values measured for thin and thick films on such alloys. In fact, the measured E_g^{opt} of thin film formed on Al-77 atom % W is noticeably higher than the theoretical one (E_g^{opt} = 3.11 eV) estimated by assuming the same cationic ratio in the alloy and into the film. According to this, a ΔE_{am} = 0.57 eV, larger than the theoretical expectation as well as that of thick film, is obtained. It seems reasonable to assume that, in the thin film range, when the anodizing process is still far from reaching the steady-state condition, the tungsten enrichment of inner mixed oxide, with respect to the base alloy, occurs at expenses of an alumina enrichment of the outer layer due to faster (than W^{6+} ions) Al^{3+} migrating ions. According to this interpretative hypothesis higher E_g^{opt} value for thin film could be attributed to an excess of aluminum ions in outer mixed layer with respect to the thicker film formed at longer anodizing times. The decrease of E_g^{opt} with increasing polarization time further confirms this hypothesis.

Finally, we want to stress that the experimental bandgap values of the investigated Al-mixed oxides confirm that the correlation proposed for d metals oxides also holds for mixed oxides containing both sp and d metals. The absence of a photoeffect for the anodized Al-15 atom % W alloy may be explained by the lower d metal content into the film, with its bandgap value then following Eq. 4. In this case, the predicted E_g^{opt} value ($\cong$5.60 eV) is above the accessible range of our experimental setup. If this interpretation is confirmed it could be inferred that a percolation threshold is necessary for using the d-metal correlation in mixed sp-d-metals oxides. Further investigation seems necessary to highlight such aspects.

Conclusions

"Mixed oxides" are formed on valve metal alloys with optical bandgap, the flatband potential and semiconducting or insulating behavior depending on the nature and relative amount of the partner oxides in the film. Thus, their solid-state properties can be controlled within a reasonably large range of values by a selection of the alloy and the anodizing process. The reported semiconducting behavior of mixed oxide grown on Al-Ti,W alloys richer in d-metal cation is appealing for tailoring transparent semiconducting oxides recently proposed in microelectronics applications.[42]

The measured bandgaps agree well with the proposed correlation with the electronegativities of the oxide constituents. Moreover, it is confirmed that the correlation proposed for d-metal oxides applies also to "mixed oxides" containing both sp and d metals provided that a minimum d metal content ($\cong$25 atom %) is present in the mixed oxide.

Concerning the V_{FB} estimate of mixed oxides, this study suggests that photocurrent spectroscopy, if correctly used, offers some advantages over Mott-Schottky plots for estimation of flatband potentials. In fact, for insulating materials (crystalline or amorphous) Mott-Schottky analysis is not accessible while for anodic films on valve metals, usually behaving as amorphous semiconductors, the frequently reported Mott-Schottky plots display a strong frequency dependence which hampers a reliable determination of flatband potential value.[43]

The Università di Palermo assisted in meeting the publication costs of this article.

References

1. H. Habazaki, P. Skeldon, G. E. Thompson, and G. C. Wood, *Philos. Mag. B*, **71**, 81 (1995).
2. H. Habazaki, P. Skeldon, K. Shimizu, G. E. Thompson, and G. C. Wood, *Corros. Sci.*, **37**, 1497 (1995).
3. H. Habazaki, P. Skeldon, G. E. Thompson, and G. C. Wood, *Philos. Mag. B*, **73**, 297 (1996).
4. H. Habazaki, K. Shimizu, P. Skeldon, G. E. Thompson, and G. C. Wood, *Proc. R. Soc. London, Ser. A*, **453**, 1593 (1997).
5. H. Habazaki, K. Shimizu, P. Skeldon, G. E. Thompson, and G. C. Wood, *Thin Solid Films*, **300**, 131 (1997).
6. H. Habazaki, K. Takahiro, S. Yamaguchi, K. Shimizu, P. Skeldon, G. E. Thompson, and G. C. Wood, *Philos. Mag. A*, **80**, 1027 (2000).
7. H. Igarashi, S. Shimizu, and Y. Kubo, *IEEE Trans. Compn. Hybrids Manufact. Technol.*, **CHM16**, 363 (1983).
8. S. Shimizu and Y. Arai, Euro. Pat. 84/102 880 (1984).
9. T. Mochizuki, Jpn. Pat. 88 306 614 (1988).
10. G. P. Chiavarotti, F. Di Quarto, M. Santamaria, and C. Sunseri, Euro. Pat. 0 966 008 A2 (22-12-1999); U.S. Pat. 6,325,831 (2001).
11. Y. Matsui, M. Hiratani, S. Kimura, and I. Asano, *J. Electrochem. Soc.*, **152**, F54 (2005).
12. C. W. Hill, G. J. Derderian, and G. Sandhu, *J. Electrochem. Soc.*, **152**, G386 (2005).
13. M. Grätzel, *Nature (London)*, **414**, 15 (2001).
14. M. Grätzel, *MRS Bull.*, **30**, 23 (2005).
15. J. O'M. Bockris and Y. Kang, *J. Solid State Electrochem.*, **1**, 17 (1997).
16. E. McCafferty, *J. Electrochem. Soc.*, **146**, 2863 (1999).
17. E. McCafferty, *Corros. Sci.*, **45**, 301 (2003).
18. F. Di Quarto, S. Piazza, C. Sunseri, and M. C. Romano, *J. Phys. Chem. B*, **101**, 2519 (1997).
19. F. Di Quarto, S. Piazza, M. Santamaria, and C. Sunseri, in *Handbook of Thin Film Materials*, Vol. 2, H. S. Nalwa, Editor, p. 373, Academic Press, San Diego (2002).
20. F. Di Quarto, M. Santamaria, and C. Sunseri, in *Analytical Methods in Corrosion Science and Technology*, P. Marcus and F. Mansfeld, Editors, p. 697, Taylor and Francis, Boca Raton, FL (2005).
21. M. Santamaria, D. Huerta, S. Piazza, C. Sunseri, and F. Di Quarto, *J. Electrochem. Soc.*, **147**, 1366 (2000).
22. H. Habazaki, M. Uozumi, H. Konno, K. Shimizu, P. Skeldon, and G. E. Thompson, *Corros. Sci.*, **45**, 2063 (2003).
23. Y. Song, X. Zhu, X. Wang, J. Che, and Y. Du, *J. Appl. Electrochem.*, **31**, 1273 (2001).
24. L. A. Fishgoit, A. D. Davydov, A. N. Kamkin, A. V. Popov, and L. L. Meshkov, *Russ. J. Electrochem.*, **33**, 1115 (1997).
25. J. P. S. Pringle, *Electrochim. Acta*, **25**, 1423 (1980).
26. S. Trasatti, in *Advances in Electrochemistry and Electrochemical Engineering*, Vol. 10, H. Gerischer and C. W. Tobias, Editors, p. 213, John Wiley, New York (1977).

27. F. Di Quarto, C. Gentile, S. Piazza, and C. Sunseri, *Corros. Sci.*, **35**, 801 (1993).
28. F. Di Quarto, S. Piazza, C. Sunseri, M. Yang, and S. M. Cai, *Electrochim. Acta*, **41**, 2511 (1996).
29. S. Piazza, A. Splendore, A. Di Paola, C. Sunseri, and F. Di Quarto, *J. Electrochem. Soc.*, **140**, 3146 (1993).
30. M. A. Butler, *J. Appl. Phys.*, **48**, 1914 (1977).
31. F. Di Quarto, A. Di Paola, and C. Sunseri, *Electrochim. Acta*, **26**, 1177 (1981).
32. A. N. Kamkin and A. D. Davydov, *Prot. Met.*, **35**, 134 (1999).
33. F. Di Quarto, C. Gentile, S. Piazza, and C. Sunseri, *J. Electrochem. Soc.*, **138**, 1856 (1991).
34. G. Tuccio, S. Piazza, C. Sunseri, and F. Di Quarto, *J. Electrochem. Soc.*, **146**, 493 (1999).
35. F. Di Quarto, A. Di Paola, S. Piazza, and C. Sunseri, *Sol. Energy Mater.*, **11**, 419 (1985).
36. N. F. Mott and E. A. Davis, *Electronic Processes in Non-Crystalline Materials*, 2nd ed. Clarendon Press, Oxford (1979).
37. L. Pauling, *The Nature of Chemical Bond*, Cornell University Press, New York, London (1973).
38. S. Piazza, L. Calà, C. Sunseri, and F. Di Quarto, *Ber. Bunsenges. Phys. Chem.*, **101**, 932 (1997).
39. A. Pignolet, G. Mohan Rao, and S. B. Krupanidhi, *Thin Solid Films*, **258**, 230 (1995).
40. S. Maeng, L. Axe, T. Tyson, and A. Jiang, *J. Electrochem. Soc.*, **152**, B60 (2005).
41. H. Habazaki, K. Shimizu, P. Skeldon, G. E. Thompson, G. C. Wood, and X. Zhou, *Corros. Sci.*, **39**, 731 (1997).
42. K. Nomura, H. Ohta, A. Takagi, T. Kamiya, M. Hirano, and H. Hosono, *Nature (London)*, **432**, 488 (2004).
43. F. Di Quarto, F. La Mantia, and M. Santamaria, *Electrochim. Acta*, **50**, 5090 (2005).